Journal of the European Ceramic Society 44 (2024) 1256–1266

Contents lists available at ScienceDirect

Journal of the European Ceramic Society

journal homepage: www.elsevier.com/locate/jeurceramsoc

Thermomechanical behavior of an alumina-mullite-zirconia refractory ceramic: sintering and thermally induced damage

Amélie Bigeard [a,b], Pierrick Vespa [b], Paul Leplay [b], Camille Mesnager [b], Olivier Citti [b], Didier Bouvard [a], David Jauffres [a,*]

[a] Univ. Grenoble Alpes, CNRS, Grenoble INP, SIMaP, 38000 Grenoble, France
[b] Saint-Gobain Research Provence, 84300 Cavaillon, France

ARTICLE INFO

Keywords:
Refractories
Alumina-Mullite-Zirconia
Sintering
Microcracking

ABSTRACT

The thermomechanical behavior of a refractory ceramic containing aggregates (particles larger than 200 μm) of alumina and mullite-zirconia, a matrix (particles smaller than 200 μm) composed of alumina, silica and zirconia and a cement binder has been investigated. Dilatometry and in-situ monitoring of mechanical properties (elastic modulus, hot strength) during different thermal treatments were performed. The evolution of the physical and mechanical properties was attributed to three main phenomena: (i) dehydration from room temperature to 800 °C, (ii) liquid phase sintering from 800° to 1350°C and (iii) microcracking during cooling. This last phenomenon was specifically studied through a comprehensive analysis of the different phases of the materials. It is shown that the main cause of microcracking was the difference of coefficients of thermal expansion between the mullite-zirconia aggregates (3.3 *10^{-6} /°C) and the matrix (7.0 *10^{-6} /°C).

1. Introduction

A sintered refractory material is defined as 'a non-metallic material or product (but not excluding those containing a proportion of metal) whose chemical and physical properties allow it to be used in a high temperature environment', according to the ISO norm ISO 836:2001 [1]. Refractories can be divided in two categories: shaped and unshaped structures. Shaped refractories, also referred to as bricks, have a definite shape, while unshaped refractories, or monolithics, such as castables or mortars, can be converted into any desired shape [2]. These refractories are designed by mixing coarse (aggregates) and fine grains (matrix) with fillers, binders, additives and water [3]. Such materials withstand severe conditions in industrial furnaces (e.g. used in steelmaking, cement, petrochemical and glass industries), such as high temperatures and thermal gradients, thermal shocks or chemical attacks (leading to corrosion). Alumina castable refractories, containing mullite-zirconia aggregates, with a calcium aluminate cement (CAC) binder, referred to as CAC bonded alumina-mullite-zirconia (AMZ) refractories, resist well to these conditions, thanks to their excellent strength, toughness and thermal shock resistance [4–6]. Although they have an important industrial role, CAC bonded AMZ refractories have not been widely studied in the literature. To improve the quality of these products or to better formulate them for specific applications it is important to deeply understand their thermomechanical properties and their microstructural evolutions during heating and cooling.

Prior to their use, thermal treatments can be applied to refractory materials to improve their strength through sintering. However, even slow and homogeneous thermal treatments sometimes lead to thermal damage, mainly in the form of microcracking, with two possible origins [7]:

- Thermal expansion mismatch between the phases;
- Physicochemical transformations, such as dehydration of the cement hydrates or zirconia phase transformation.

In the case of thermal expansion mismatch between phases, Fogaing et al. [7] proposed a simplified model of microcracking during cooling. They considered a two-phase material, composed of spherical inclusions, with a coefficient of thermal expansion (CTE) α_p, embedded in an isotropic homogeneous matrix, with a CTE of α_m. Depending on the difference of CTE, $\Delta\alpha = \alpha_m - \alpha_p$, three configurations may occur during cooling:

* Corresponding author.
E-mail address: david.jauffres@grenoble-inp.fr (D. Jauffres).

https://doi.org/10.1016/j.jeurceramsoc.2023.09.051
Received 19 June 2023; Received in revised form 12 September 2023; Accepted 21 September 2023
Available online 23 September 2023

- $\Delta\alpha < 0$: the matrix CTE is lower than the inclusion CTE. Cooling generates orthoradial compressive and radial tensile stresses in the matrix and at the interface that induce either partial or complete decohesion, depending on the stress magnitude.
- $\Delta\alpha = 0$: perfect expansion agreement, no stress is expected.
- $\Delta\alpha > 0$: the matrix CTE is greater than that of the inclusion. During cooling, orthoradial tensile and radial compressive stresses are generated, resulting in the formation of radial cracks in the matrix, around the inclusion.

Tessier-Doyen [8] and Huger et al. [9] developed model materials to investigate this phenomenon. The model materials were composed of a borosilicate glass matrix with a tunable CTE mixed with mono diameter spherical alumina particles. They plotted the evolution of the modulus of elasticity (MOE), or Young's modulus, as a function of temperature for the two extreme cases ($\Delta\alpha < 0$ and $\Delta\alpha > 0$), and compared the values with the lower bound of the Hashin and Shtrikman (HS) model [10]. This model based on the theory of linear elasticity provides upper and lower bounds for the effective elastic moduli of a matrix-inclusion homogenized medium with isotropic constituents [10]. According to Huger [11], the lower bound was often the most relevant in defect-free materials containing rigid inclusions and a soft matrix. In both cases, during cooling, the Young's modulus follows the lower HS bound until 200–300 °C. The MOE significantly decreases at lower temperatures and depart from the HS bound that remains stable, indicating damage in the material. This decrease is much more pronounced for $\Delta\alpha > 0$, which the authors explain by the higher surface of defects involved in radial microcracking around the inclusions of the material [9]. It is worth noting that once properly comprehended, the microcracking phenomenon, at first view detrimental, can be controlled and used to enhance thermal shock resistance [9,12–14].

These theoretical and model assertions were also observed experimentally on industrial products. Ferrari et al. [15] mentioned the occurrence of microcracking in an AMZ refractory, but they did not specifically focus on the causes and consequences of such a behavior. Chotard et al. [16] investigated this phenomenon in more details in a cordierite mullite refractory. In their paper, the authors attributed the microcracking effect to the thermal expansion mismatch between the cordierite matrix (1.5 – 3 *10^{-6} /°C) and the mullite grains (4 – 6 *10^{-6} /°C), which generated internal stresses, leading to microcracks and decohesion during cooling. Kakroudi et al. [12] compared two refractory castables, containing respectively andalusite and bauxite aggregates. Both refractories are subjected to damage during cooling, with a marked decrease of their elastic properties, due to the thermal expansion mismatch between the aggregates and the matrix. Nevertheless, the phenomenon is much more pronounced in the andalusite refractory, due to the thermal expansion anisotropy of an andalusite single crystal [17]. Indeed, Kakroudi et al. observed a large difference between the coefficients of thermal expansion (CTE) of the matrix (7.6 *10^{-6} /°C) and the different directions in the andalusite crystal (12.9 *10^{-6} /°C for axis $\vec{a}$ and 3.1 *10^{-6} /°C for axis $\vec{c}$). This difference of behavior between the bauxite and andalusite refractories is in agreement with the tensile tests performed after thermal treatment by the authors, which show a more extended non-linear behavior in the andalusite material.

The microcracking phenomenon can also be observed in dilatometry tests [16,18,19]. Mouiya et al. [18] studied in detail the evolution of the deformation of an aluminium titanate based (AT) material doped with silica. During heating, the rate of expansion was related to microcrack healing (slow rate) or closure (higher rate). During cooling, two stages were observed: thermal contraction in the first stage and expansion from 750 °C, due to microcracks opening. The authors were also able to estimate the volume fraction of microcracks at room temperature (2.4 vol % in their material).

In the case of zirconia containing refractories, another level of complexity is brought by the monoclinic (m) - tetragonal (t) and t-m phase changes occurring respectively around 1150 °C during heat up and 1000 °C during cooling [20,21]. In addition to a direct effect due to the lower elastic modulus of the tetragonal phase, an indirect effect is possible through the large volume change (around 4% in the case of pure zirconia), which can induce microcracking as well [22–25].

The physico chemical transformations in the material also play a major role in the evolution of damage in a refractory castable. Today, calcium aluminate cement (CAC) is the most used binder in refractory castables compositions, as it provides high green mechanical strength, appropriate setting time and good corrosion resistance [26–28]. CAC is composed of many calcium aluminate phases that hydrate with water, based on a dissolution/precipitation reaction, at low temperatures, providing green strength to the castable refractory [29,30]. During heating, the progressive decomposition of the hydrated phases leads to degradation of the chemical bonds and porosity increase, resulting in drastic decrease of the mechanical properties of the refractory [30–34]. For instance, in the case of alumina refractories dried at 110 °C for at least 24 h, the MOE dropped from 20 to 10 GPa for 5.5 wt% of cement and 5 wt% of water [34] and from 100 to 60 GPa for 4 wt% of cement and 4.4 wt% of water [33].

In this context, the objective of this study is to understand the mechanisms of consolidation and damage during high temperature cycles of an alumina-mullite-zirconia refractory. This material was prepared with a calcium aluminate cement binder. The evolution of physical (density, porosity, crystal phases), thermal (thermal expansion) and mechanical (modulus of elasticity, flexural strength) properties as a function of temperature was studied. Furthermore, the refractory, the aggregates and the matrix properties were also separately studied to allow an in-depth analysis of the roots of the microcracking phenomenon in the refractory.

2. Materials and methods

2.1. Material and sample preparation

The specimens were fabricated by mixing aggregates, larger than 200 μm (~70 wt%), with matrix particles, smaller than 200 μm (~30 wt %). Three castable refractories were prepared as follows.

- In the material that was mostly investigated, called 'mat_MZ', aggregates were composed of mullite-zirconia and alumina grains while the matrix contained alumina, silica and zirconia particles with calcium alumina cement (CAC) as a binder. A dispersant was added to adjust the viscosity of the mixture. The viscosity was determined with a Lamy rheology Couette viscosimeter with a shear stress of 2.6 Pa. All raw materials were mixed in a Perrier planetary mixer for 15 min. The mixture was then cast into bar-shaped molds of size 150 * 25 * 25 mm^3. After 6 h, the parallelepiped bars were demolded and cured at ambient temperature for approximately 24 h. Finally, the specimens were oven-dried at 250 °C.
- In the second formulation, called 'mat_Al', mullite-zirconia aggregates were replaced by alumina aggregates with the same particle size distribution. The same protocol was followed for the other steps.
- In the last formulation, called 'mat_Mul', mullite-zirconia aggregates were replaced by mullite aggregates, with the same particle size distribution. The same protocol was followed for the other steps.

Table 1 details the formulations of the studied materials.

An additional formulation containing only the matrix and dispersant was prepared using identical methodology. The water content was adjusted to obtain an adapted rheology.

2.2. Physical characterization

The casted specimens were characterized for bulk density and open

Table 1
Compositions of the three studied refractory castables, 'mat_MZ', 'mat_Al' and 'mat_Mul'.

Raw materials	Size	Content in 'mat_MZ' (wt %)	Content in 'mat_Al' (wt %)	Content in 'mat_Mul' (wt %)
Mullite zirconia	3–0 mm	25	-	-
Mullite	3–0 mm	-	-	25
Tabular alumina	3–0 mm	44	69	44
Matrix (alumina + silica + zirconia)	< 200 μm	28	28	28
Calcium aluminate cement	< 100 μm	3	3	3
Dispersant	-	< 1	< 1	< 1
Water	-	7	7	7

porosity by Archimedes immersion technique with water as the immersion fluid, according to standard DIN EN 623–2. The closed porosity was measured by Helium pycnometry by comparing the porosity on the solid sample and on the crushed sample.

2.3. Thermal characterization

Dilatometry experiments up to 1350 °C with 1 h dwell time, using 100 °C/h heating and cooling rates, were performed with specimens core drilled as cylinders (50 mm height and external diameters and 12 mm central inner diameter) according to Afnor standard NF EN 993–19. Dilatometry tests were also performed on aggregates, specifically chosen with a flat lower surface. In this case, norm ASTM E 831 was followed. The evolution of the deformation versus temperature and the coefficient of thermal expansion of the specimens have been measured. The coefficient of thermal expansion of the material was deduced from the dilatometric tests.

2.4. Thermomechanical characterization

The Modulus Of Elasticity (MOE), or Young's modulus, was measured by IMCE NV [35] with bars of dimensions 150 * 25 * 25 mm^3 by the impulse excitation technique, using a laser doppler vibrometer to capture the signal. In this technique, the doppler effect between a reference laser beam and the laser beam reflected by the sample gives the displacement of the sample surface and the resonance frequency [36]. A laser doppler vibrometer is more sensitive than a traditional microphone and offers high quality signals, especially at high temperatures. Continuous measurements were performed up to 1350 °C, with heating and cooling ramps of 200 °C/h and a dwell time of 2 h. The elastic modulus was calculated with the ASTM E1816–01 formula [37]:

$$E = 0.9465 * \frac{m * f_r^2}{b} * \left(\frac{L}{t}\right)^3 * C_f$$

With E the elastic modulus (Pa), m the mass of the bar (g), f_r the fundamental resonant frequency of the bar in flexure (Hz), b, L and t the width, length and thickness of the bar respectively (mm) and C_f the correction factor for the fundamental flexural mode, that accounts for finite thickness and Poisson ratio of the specimen. Simultaneously to this MOE test, the energy dissipation during vibration or impact can be measured through the damping factor of the signal. It can be correlated to the internal friction in the material [38].

The hot strength, defined here as the maximum stress reached in the specimens during a three-point bending test (span 120 mm), was evaluated based on ASTM C583 standard. Tests were made with bars of 150 * 25 * 25 mm, at different temperatures, up to 1350 °C, with a heating rate of 200 °C/h and one hour dwell time for each temperature. At 1350 °C, the test was performed after 1, 2 or 10 h. Additionally, some specimens were heated up to 1350 °C (2 h dwell time) and then cooled down to a specific temperature, with a cooling rate of 200 °C/h. Hot strength was measured at that temperature after 1 h dwell time at each temperature. Examples of these experimental conditions are given in Fig. 1. The displacement rate was 0.5 mm/min. Two cycles were performed, each value corresponding to the average of 4 or 3 tests for the first and second cycles respectively. The indicated dwell time corresponds to the time at which the first bar was tested. The other bars were then tested every 15 min. Standard deviation have been plotted as error bars on the graphs.

2.5. Microstructural characterization

The microstructure of the specimens was characterized by field emission scanning electron microscopy (FEG Zeiss Ultra 55) on polished surfaces of epoxy-resin infiltrated samples.

2.6. Chemical and structural characterization

Specimens were ball-milled and the resulting powders were submitted to:

- Chemical analyses, carried out by X-Ray fluorescence (XRF), performed with a Zetium device, from Malvern Panalytical.
- Phase analyses, by X-Ray powder diffraction (XRD), performed with a D8 Endeavor device from Bruker, and quantified according to Rietveld method. XRD measurements were made at room temperature and during a temperature cycle with heating and cooling rates of 10 °C/min, 15 min of stabilization and 15 min of measurement at each temperature.

3. Results

3.1. Composition and phases

The viscosity of the prepared mixture was measured as 8 Pa.s. The bulk density of the refractory 'mat_MZ' is 2.991 ± 0.004 g/cm^3 and the open porosity is 17.7 ± 0.1%. The closed porosity is negligeable in the material (<1%). The chemical composition and the phases of 'mat_MZ' are presented in Table 2 and Table 3, respectively.

It is noteworthy that the reaction of these different compounds can lead to the formation of new phases [7]. In this article, 'liquid phases' will refer to both:

- the appearance of new phases during heating and originating from the presence of impurities that react with raw materials and favor the formation of eutectics with low melting points, e.g. alumina reacting with lime (CaO), present in CAC.
- the softening of amorphous phases, initially present in the material, e.g. silica.

During cooling, the low-melting point eutectics and the phases resulting from fine particles reacting together will solidify, while the amorphous phases will stiffen. These phenomena will be grouped under the term 'solidification of liquid phases'.

The in-situ XRD measurements showed a clear zirconia phase change during heating, between 1100 and 1200 °C (monoclinic to tetragonal), as illustrated by Fig. 2. During cooling, the reverse phase change (tetragonal to monoclinic) is more progressive and spreads from 1000° to 500°C (Fig. 3).

The microstructure of a polished section of the material 'mat_MZ' is shown in Fig. 4. This multi-scale material contains:

- Aggregates of mullite-zirconia, an electro fused bi-phase ceramic that appears light grey (mullite) and white (zirconia),
- Aggregates of alumina that appears in a darker grey,

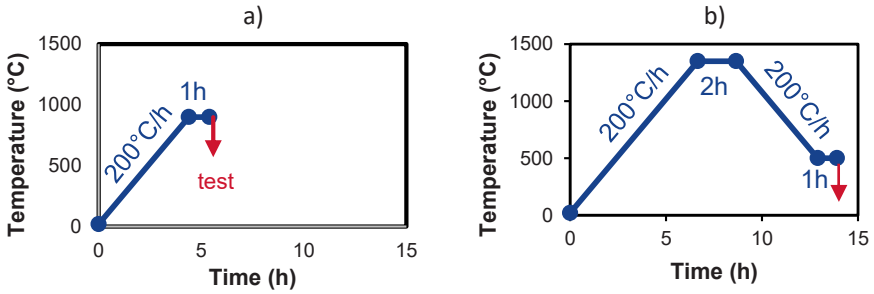

Fig. 1. Two examples of thermal treatment applied to the specimens before flexural test, for hot strength measurement. a) Test performed after a heating ramp of 200 °C/h until 900 °C with a dwell time of 1 h. b) Test performed after a heating ramp of 200 °C/h until 1350 °C with a dwell time of 2 h, followed by cooling at 200 °C/h until 500 °C with a dwell time of 1 h.

Table 2
Chemical analysis of the refractory castable.

Compounds	Amount in refractory (wt%)
Al_2O_3	75
ZrO_2	12
SiO_2	10
CaO	< 1
MgO	< 1
Na_2O	< 1

Table 3
Main phases of the refractory castable.

Phases	Amount in refractory (wt%)
Corundum	67
Mullite	19
Monoclinic zirconia	11
Alumina β	3

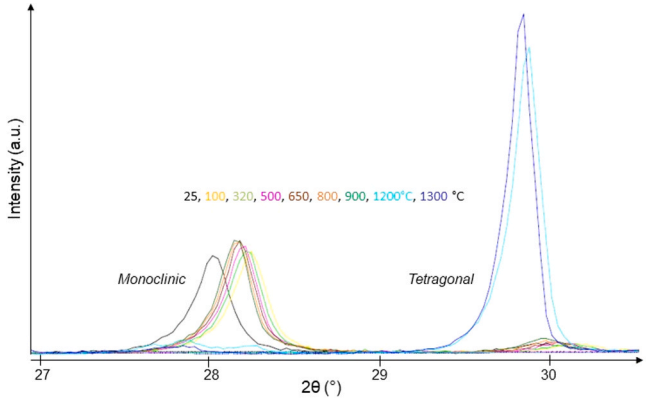

Fig. 2. Evolution of the XRD peaks of the monoclinic (left) and tetragonal (right) zirconia during heating with a heating rate of 10 °C/min, in the range 27–30.5°.

- A matrix that contains finer alumina, zirconia and silica particles that appear in grey-scale.
- Pores appear in black as they are filled with epoxy resin. It is worth noting that only macroporosity is visible at this scale but microporosity is also present in the material.

3.2. Dilatometry

The results of the dilatometry tests for the refractory 'mat_MZ' are displayed in Fig. 5. Two successive heating / cooling cycles up to 1350 °C are shown. During the first cycle, the specimen exhibits a linear

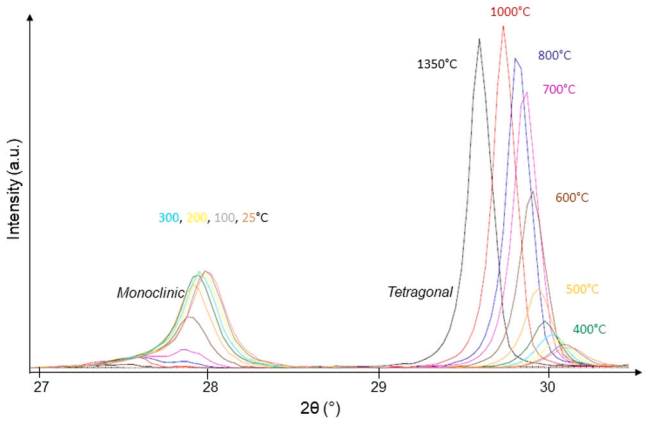

Fig. 3. Evolution of the XRD peaks of the monoclinic (left) and tetragonal (right) zirconia, during cooling at 10 °C/min in the range 27–30.5°. The powders were first heated at 60 °C/min up to 1350 °C.

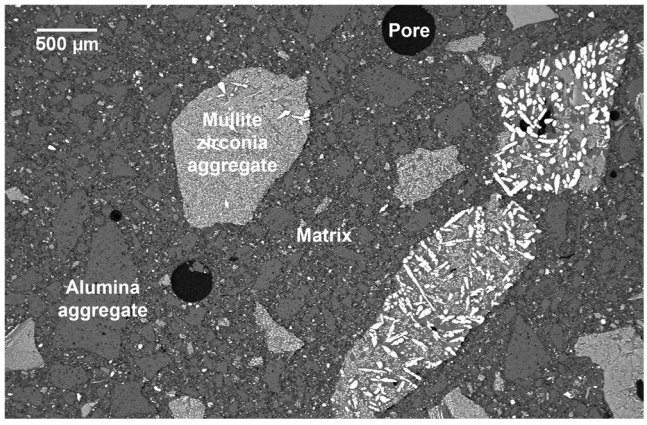

Fig. 4. SEM microstructure of the studied material. Zirconia appears in white, mullite in light grey, alumina in medium grey and pores in black.

thermal expansion up to 1300 °C, reaching a deformation of 0.8% before showing a slight shrinkage (0.1%). During the dwell time, the material shrinks by 0.1%. During cooling, the material contracts and two inflections can be distinguished around 1000 and 750 °C. Afterwards, the shrinkage of the material continues. The final deformation of the material is 0.03%. The curve in the second cycle is very similar during cooling but it shows some marked differences during heating: a decrease of the apparent coefficient of thermal expansion (CTE) between 800 °C and 1150 °C, an extra drop around 1150 °C and no or very limited shrinkage at high temperature and during the dwell. A third cycle was

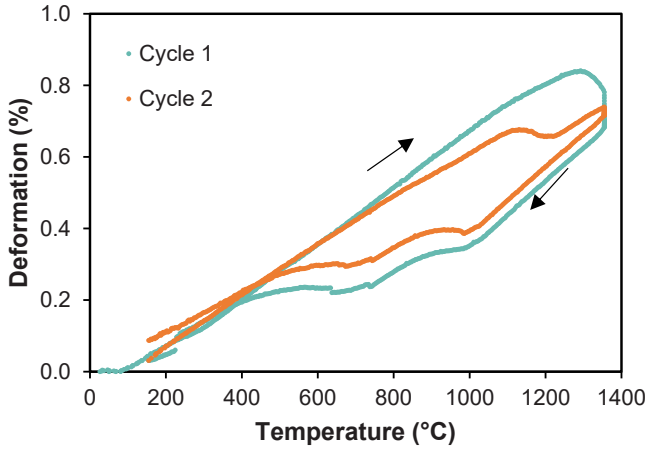

Fig. 5. Deformation of the 'mat-MZ' vs temperature, during two successive cycles, up to 1350 °C, with heating and cooling rates of 100 °C/h and a dwell time of 1 h.

performed, which was similar to the second one.

In Fig. 6, the deformation of the matrix is represented as a function of temperature. The specimen expands from 400° to 900°C, reaching a maximum deformation of 0.3%. A shrinkage is next observed, mainly between 1300 and 1350 °C after 1 h dwell time. During cooling, a linear shrinkage is observed. The final deformation is − 4.5%, which corresponds to a volume shrinkage of − 13.5%. The CTE, measured between 600 and 200 °, was assessed to be 7.0 * 10^{-6} /°C.

In Fig. 7, the deformations of an alumina (a), a mullite (b) and a mullite-zirconia (c) aggregate are represented as a function of temperature. In Fig. 7a, the alumina grain shows a linear thermal expansion up to around 1% at 1350 °C. During cooling, a linear thermal contraction is observed as well, with a total shrinkage of less than 0.2% after the thermal treatment. The CTE of the aggregate, measured during cooling between 600 and 200 °C, equals 8.5 * 10^{-6} /°C, in line with the expected value for α-alumina [39]. In Fig. 7b, the mullite aggregate exhibits a linear thermal expansion up to 0.7% at 1350 °C. During cooling, the linear thermal contraction leads to a total shrinkage of less than 0.2%. The CTE of the aggregate, measured during cooling between 600 and 200 °C, is 5.1 * 10^{-6} /°C, a value that is consistent with literature [16]. In Fig. 7c, the expansion of the mullite-zirconia aggregate during heating is interrupted by an abrupt shrinkage around 1100 °C (−0.5%). During cooling, the material slightly shrinks, except in the range 1000–800 °C, that shows a progressive expansion of 0.4%. The CTE of the aggregate, measured during cooling between 600 and 200 °C, equals

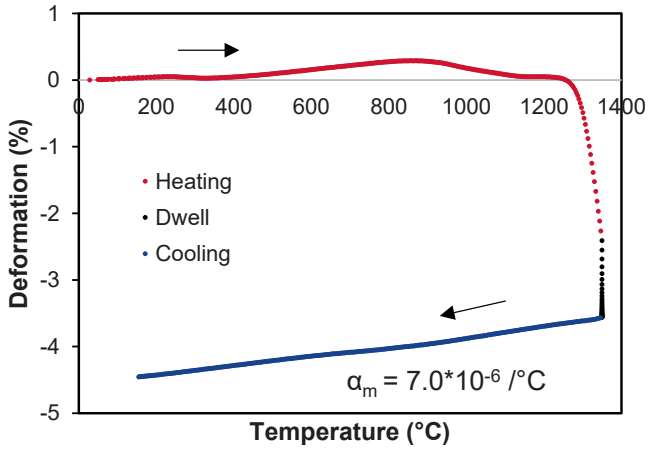

Fig. 6. Deformation of the matrix vs temperature in a cycle up to 1350 °C with heating and cooling rates of 100 °C/h and a dwell time of 1 h.

3.3 * 10^{-6} /°C. This behavior and the CTE value are consistent with previous work [40]. These dilatometry tests were repeated with other aggregates and the same behavior was observed.

3.3. Hot modulus of elasticity

Fig. 8a shows the in-situ evolution of the elastic modulus of 'mat_MZ' during three successive heating-cooling cycles up to 1350 °C. All curves describe a hysteresis loop. The initial MOE value is 32 GPa and, during the first heating cycle, a gradual decrease, down to 22 GPa, is observed until around 800 °C. Then, from 800° to 1200°C, the modulus strongly increases up to approximately 60 GPa, before dropping again until 1350 °C. The absence of points from 900° to 970°C in the first HMOE cycle comes from a technical issue, with the tapping device blocking in this temperature range. The modulus continuously increases during the two-hour dwell time and during cooling down to 1000 °C, to reach a value close to 100 GPa. Two inflections are next observed, slightly below 1000 °C and around 750 °C. Finally, the modulus of elasticity continuously decreases down to room temperature. The final value (49 GPa) is 44% higher than the initial one. During the second cycle, the elastic modulus remains stable up to 800 °C. A slight inflection is observed around 900 °C, before an increase until 1200 °C and a final drop similar to the one observed during the first cycle. During the dwell time, the MOE increase is much lower than during the first cycle. The cooling part is similar to the one of the first cycle. The third cycle shows an evolution alike the second cycle. Fig. 8b provides additional information, with the evolution of the damping factor during the first cycle. During heating, the damping factor is close to zero until 800 °C. Above this temperature, the factor increases up to 0.3 at 1350 °C. During the dwell time, it drops to 0.2, before continuously decreasing during cooling. Around 900 °C, this parameter is close to zero again.

The influence of the maximum temperature reached during a thermal treatment on the MOE of 'mat_MZ' is presented in Fig. 9. Every thermal treatment was performed on a dried specimen at 200 °C/h, with two-hour dwell time. Four heating / cooling cycles are presented here, with maximum temperatures of 700, 1000, 1100 and 1200 °C. During heating, all specimens show a decrease of the modulus at low and intermediate temperatures (up to ~800 °C). After the thermal treatment at 700 °C, the MOE continues its decrease during cooling down to room temperature. For other temperatures, the elastic modulus starts increasing at 800 °C and continues during the two-hour dwell time. During cooling, after a plateau, all specimens show a decrease of the modulus below 750 °C.

The effect of the dwell time on the evolution of the HMOE of 'mat_MZ' refractory castable was measured as well and is displayed in Fig. 10. The elastic modulus continuously rises during the dwell time, from 20 to 43 GPa, with a steeper slope during the first hours.

Fig. 11 plots the evolution of the hot MOE of specimen 'mat_Al', compared with 'mat_MZ'. The initial MOE value is higher for 'mat_Al', close to 40 GPa. During heating, both materials have similar evolutions, with a higher rise from 900° to 1200°C for 'mat_Al' though. During cooling however, the HMOE slightly increases from around 90 GPa at 1200 °C to more than 100 GPa back to room temperature. This behavior is very different from the decrease below 750 °C observed in 'mat_MZ'.

The evolution of the hot elastic modulus of specimen 'mat_Mul' is plotted in Fig. 12. The initial MOE value is close to 40 GPa. Then the evolutions of the elastic modulus during heating and cooling are similar with those of the reference 'mat_MZ'. During heating, a decrease of the modulus until 800 °C and a rise up to 70 GPa at 1200 °C can be observed. During cooling, a continuous increase of the elastic modulus until 700 °C is followed by a drop with a final value of 60 GPa at room temperature.

Finally, the evolution of the MOE of the matrix as a function of temperature is displayed in Fig. 13. During heating, the evolutions are close to the ones observed in the refractory: the MOE decreases from around 20 GPa at room temperature to 15 GPa at 800 °C, rises up to

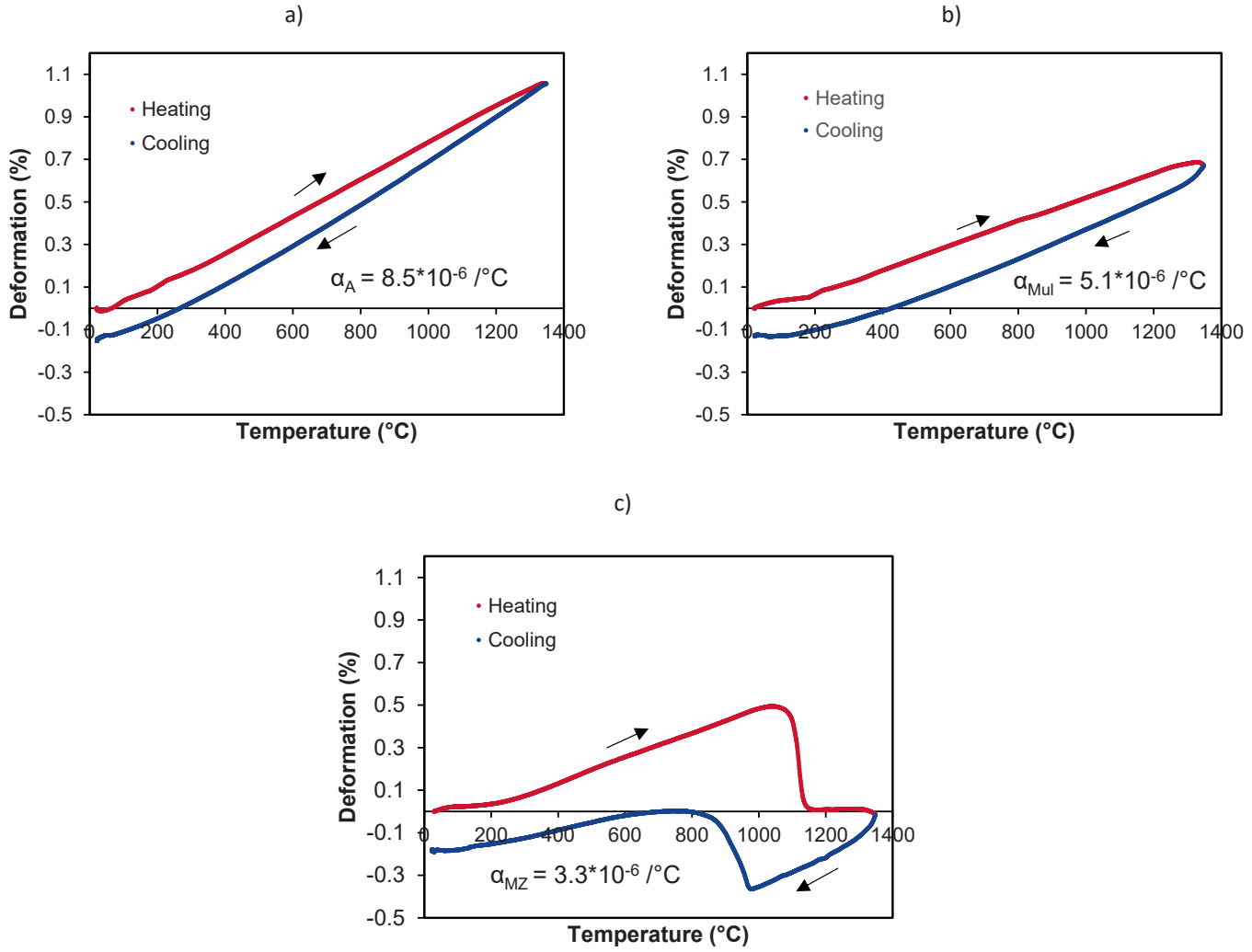

Fig. 7. Expansion and shrinkage vs temperature in a cycle up to 1350 °C with heating and cooling rates of 10 °C/min and no dwell time of a) an alumina aggregate (A), b) a mullite aggregate (Mul), c) a mullite-zirconia (MZ) aggregate.

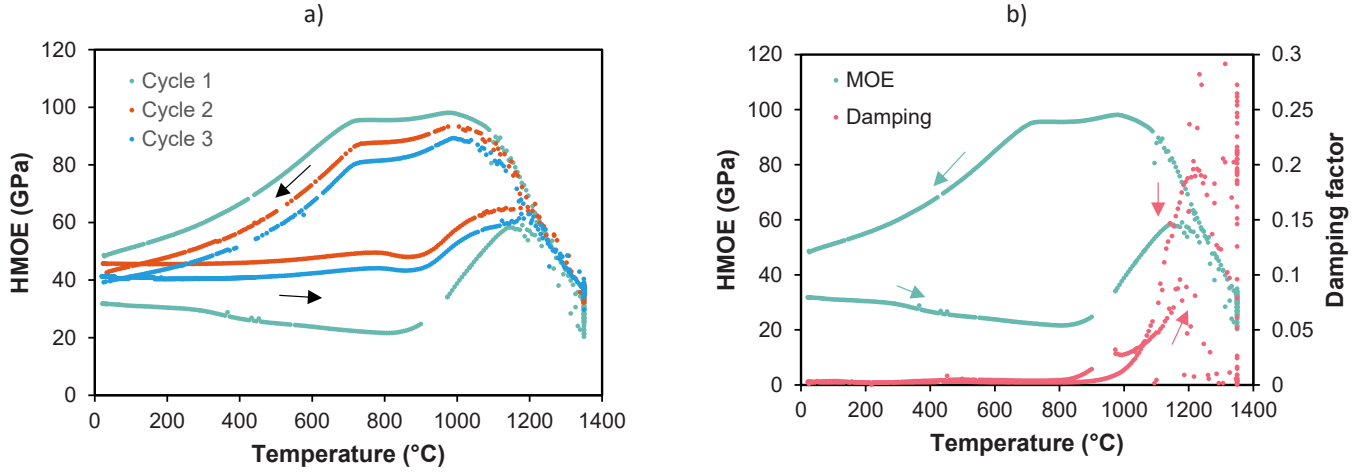

Fig. 8. Evolution of the properties of 'mat_MZ' in a cycle up to 1350 °C, with heating and cooling rates of 200 °C/h and a dwell time 2 h. a) Hot modulus of elasticity during three successive cycles b) Hot modulus of elasticity and associated damping factor during the first cycle.

1200 °C and drops down until 1350 °C. During the two-hour dwell time, the elastic modulus continuously increases and this rise continues during the beginning of cooling, reaching 97 GPa at 1100 °C. The abrupt loss at 900 °C, from 100 to 94 GPa, is likely due to experimental conditions and do not reflect a specific phenomenon in the material. From 900 °C down to room temperature, the behavior of the matrix is

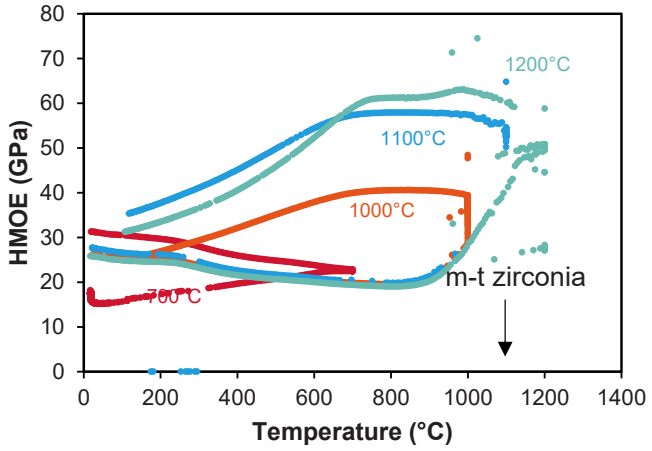

Fig. 9. Effect of the thermal treatment on the elastic modulus of 'mat_MZ'. Maximum reached temperatures are 700 (red curve), 1000 (orange curve), 1100 (blue curve) and 1200 °C (green curve).

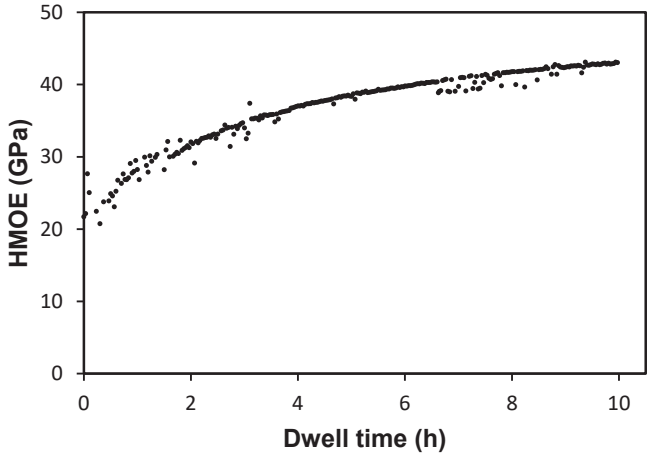

Fig. 10. Evolution of the hot modulus of elasticity of 'mat_MZ' during a ten-hour dwell time (first cycle) at 1350 °C. The specimen was heated with a rate of 200 °C/h.

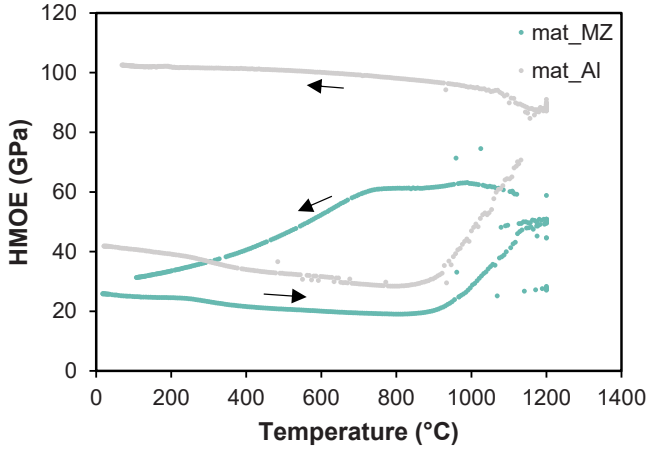

Fig. 11. Evolution of the hot modulus of elasticity of the refractory castable 'mat_Al' (mullite-zirconia grains replaced by alumina grains) in a cycle up to 1200 °C, with heating and cooling rates of 200 °C/h and dwell time 2 h.

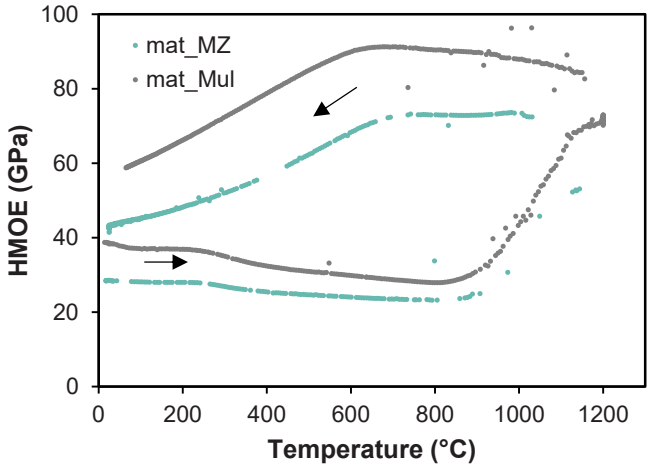

Fig. 12. Evolution of the hot modulus of elasticity of the refractory castable 'mat_Mul' (mullite-zirconia grains replaced by mullite grains) in a cycle up to 1200 °C, with heating and cooling rates of 200 °C/h and dwell time 2 h.

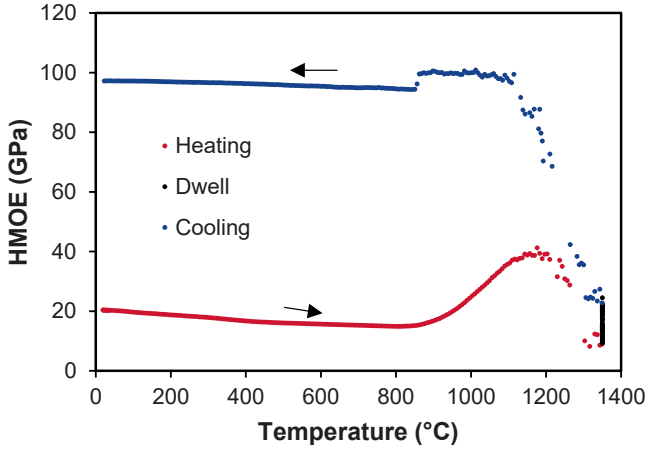

Fig. 13. Hot modulus of elasticity of the matrix, up to 1350 °C, with heating and cooling rates of 200 °C/h and dwell time 2 h.

radically different than that of the 'mat_MZ' refractory: the elastic modulus slowly increases and reaches 97 GPa.

3.4. Hot strength

Fig. 14 depicts the evolution of the hot strength of 'mat_MZ' up to 1350 °C, during two successive heating-cooling cycles. The initial strength of the refractory ceramic is 5 MPa. During the first heating, the hot strength stays low, with a slight tendency to decrease until 700 °C and to slowly increase from 900° to 1200°C. The value significantly drops at 1350 °C but it rises back during cooling, reaching 48.4 MPa at 900 °C. In the final part of the cycle, the hot strength strongly drops down to 15 MPa at room temperature. Nevertheless, the final value is three times higher than the initial one. During the second cycle, the hot strength remains stable, around 15 MPa, then it decreases from 1000° to 1350°C, reaching 2 MPa. During cooling, the hot strength reaches a maximum value of 41 MPa, which is lower than the peak of the first cycle. Finally, the strength continuously decreases down to room temperature and the final strength of the material is 13 MPa, only slightly lower than the value obtained after the first cycle.

The influence of the dwell time on the hot strength was also assessed (Fig. 15). At 1350 °C, the hot strength evolved from 2.8 to 3.8 MPa after dwell times of 1 and 10 h, respectively.

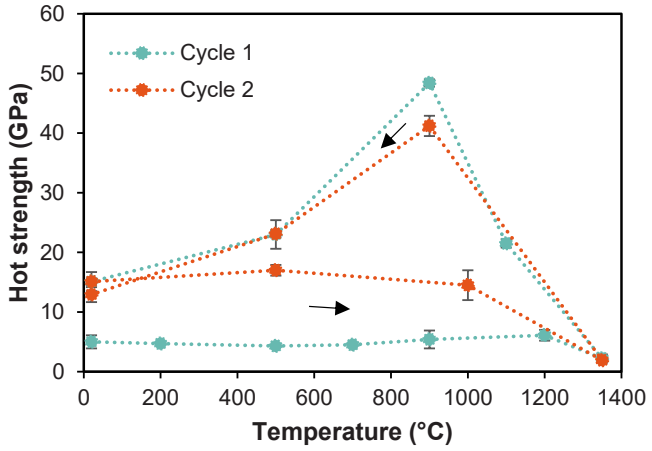

Fig. 14. Hot strength of the studied refractory castable, during two successive cycles. Testing temperatures: during heating, 20, 200, 500, 700, 900, 1200 after 1 h dwell time. 2 h dwell time at 1350 °C. During cooling, 1100, 900, 500, 20 °C after 1 h dwell time. The error bars correspond to two standard deviations.

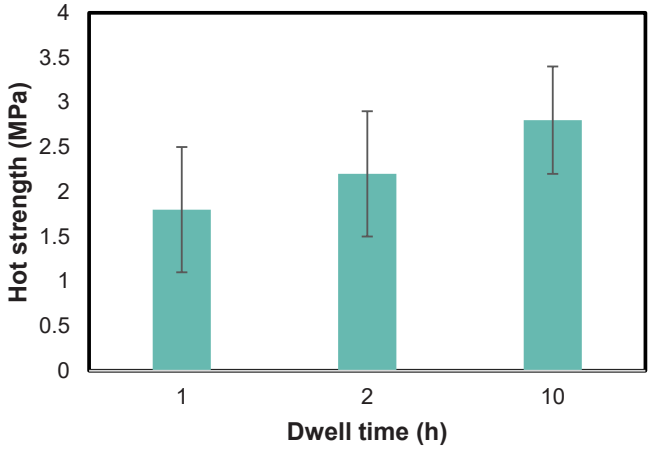

Fig. 15. Influence of the dwell time (1, 2 and 10 h) on the hot strength of the refractory, at 1350 °C. The error bars correspond to two standard deviations. The specimen was heated with a rate of 200 °C/h.

4. Discussion

4.1. General material evolution scenario during thermal cycles

The variations with temperature of the previously described properties (elastic modulus, strain, strength) are supposed to be closely related to the microstructural changes in the 'mat_MZ' refractory material. These evolutions have been divided in five stages and their interpretations are proposed below.

4.1.1. Stage 1 (heating from room temperature to 800 °C): dehydration

At low and intermediate temperatures, from 20° to 800°C, the gradual decrease of the HMOE and of the hot strength, in Fig. 8a and Fig. 14 respectively, corresponds to a mechanical degradation of the material, due to the decomposition of the hydrates contained in the binder (calcium aluminate cement). According to Thermogravimetric analysis measurements (see supplementary figure), the hydrates are fully decomposed around 800 °C, which is consistent with the second cycle, that shows a stable evolution of the MOE in the same temperature range. The dilatometry test in Fig. 5 shows a thermal expansion in this temperature range.

4.1.2. Stage 2 (heating from 800° to 1200°C): liquid phase sintering without shrinkage

From 800° to 1200°C, the elastic modulus strongly increases and the hot strength slightly rises as well. In the first cycle, this rise probably corresponds to early sintering, without shrinkage (see Fig. 5), promoted by the liquid phases. The appearance of these liquid phases is supported by the significant increase of the damping factor above 850 °C, illustrated in Fig. 8b. Plus, it is in agreement with the slight drop around 800 °C in the second HMOE heating cycle, that can be attributed to the glass transition of the amorphous phases [7] (hidden by the dehydration in the first cycle). Sintering is expected to promote consolidation and thus a concomitant increase of elastic modulus and strength. The rise is however far less large in the hot strength measurement (static test) than in the HMOE test (dynamic test). A possible origin lies in the viscous behavior of glassy phases that react differently during fast loading and small strains (dynamic), compared to slow loading and large strains (static) [41,42].

In this temperature range, other phenomena can be highlighted but they are not predominant. They were confirmed by in-situ XRD experiments.

- The crystallization of CA_2 ($CaAl_4O_7$ or grossite) at 800 °C is expected to decrease the elastic modulus of the material [43] but the proportion of this phase is very low and its effect is not observed here.
- The monoclinic to tetragonal zirconia phase transformation at 1130 °C could decrease the MOE of the material and result in strong shrinkage in the dilatometry tests. But neither a MOE loss nor a shrinkage of the material are observed. It may be related to the fact that the material is not fully sintered yet and can therefore accommodate the variation generated by the zirconia phase change, by particle rearrangement. This is coherent with the second cycle of dilatometry in which the zirconia phase change is clearly visible (Fig. 5), as the material is almost fully sintered. However, in the second cycle of MOE, no decrease is observed around 1130 °C, meaning that the phase change is hidden by another phenomenon, described later in the paper.

4.1.3. Stage 3 (heating from 1200° to 1350°C and dwell time): liquid phase sintering with shrinkage

Above 1200 °C, the strong decrease of the mechanical properties (Fig. 8a and Fig. 14) and a concomitant large increase of the damping factor (Fig. 8b) support the presence of liquid phases. The sintering is amplified by the presence of liquid phases and, above around 1300 °C, a shrinkage of the material is observed and continues during the dwell time (Fig. 5). However, the shrinkage remains low (0.1% during the dwell time at 1350 °C), which can be explained by the multiscale composition of the refractory. Indeed, the shrinkage (around −4.5%, Fig. 6) of the sintering matrix does not result in a significant macroscopic shrinkage of the refractory, as it is hindered by the presence of large aggregates [44–47]. Still, a local shrinkage of the matrix is expected, leading to mesoporosity opening [46,47]. During the dwell time at 1350 °C, the continuous MOE and hot strength increase confirm the sintering of the refractory, which requires several hours to be completed according to Fig. 10 and Fig. 15. The rise is more accentuated in the elastic modulus than in the hot strength, which is related to the viscous behavior of the liquid phases, as previously explained.

4.1.4. Stage 4 (cooling from 1350° to 800°C): stiffening

During cooling, the effect of previous sintering, combined with the solidification of liquid phases, results in a significant increase in the HMOE and the hot strength. The elastic modulus reaches a maximum around 1000 °C, temperature at which no more liquid phases are present in the material. This is coherent with the damping factor that goes back to zero around 1000–900 °C. Then, below 1000 °C, the HMOE decrease appears to be due to the progressive tetragonal-monoclinic zirconia phase change, as confirmed by the XRD measurements in Fig. 3 and the

dilatometry test in Fig. 5. The monoclinic phase has a higher Young's modulus than the tetragonal one, hence this behavior is understood as an indirect effect due the damage induced by the volumetric expansion during the phase change [24].

4.1.5. Stage 5 (cooling from 800 to room temperature): thermally induced damage

Below 750 °C, the elastic modulus and the hot strength both undergo a sharp decline down to room temperature, which is likely due to damage undergone by the material. In addition, the dilatometry test displays an inflection around 750 °C, that can also be related to microcracking, as proposed by Mouiya et al. [18] on an aluminium titanate based material.

4.2. Origin of thermally induced damage

In order to investigate the origins of damage in this complex material, the matrix and the aggregates were separately studied. Fig. 6 and Fig. 13 respectively show the evolutions of the deformation and the MOE in the matrix. During cooling, the behavior of the matrix is radically different from that of the refractory behavior, as no continuous decrease (MOE) or step (dilatometry) are observed below 750 °C. It can be deduced that, after sintering, no damage occurs in the matrix when it does not include the aggregates. Therefore, it is deduced that microcracking comes neither from physico-chemical transformations inside the matrix (dehydration / crystallizations in the binder, mullitization, zirconia phase change) nor from the differences of CTE between the constituents of the matrix.

The role of the aggregates in the material was questioned as well. In order to distinguish the respective influence of the alumina and the mullite-zirconia aggregates, 'mat_Al', containing only alumina aggregates, was specifically formulated. The comparison of the MOE evolution between materials 'mat_MZ' and 'mat_Al' is presented in Fig. 11. Two radically different behaviors are observed during cooling: while significant MOE decrease is noticed for 'mat_MZ', no loss of MOE is observed in 'mat_Al', suggesting that alumina aggregates alone do not induce microcracking. Consequently, microcraking is necessarily linked to the presence of MZ aggregates. A possible cause of microcraking, already identified as such in other materials [25,48], is the zirconia phase change occurring in the mullite-zirconia grains. This option was investigated with the comparison between the reference 'mat_MZ' and 'mat_Mul', in which mullite-zirconia grains were replaced by mullite grains, i.e. a formulation without zirconia in the aggregates. As shown in Fig. 12, MOE decrease is observed during cooling in both formulations. It can be deduced that the impact of the zirconia phase change in the mullite-zirconia aggregates is not preponderant in the microcracking phenomenon. In addition, the evolution of the MOE depending on the thermal treatment applied was plotted in Fig. 9. During cooling, all four specimens present an elastic modulus decrease from 750 °C (or 700 °C in the case of the thermal treatment going up to 700 °C), independently of the maximum temperature reached. More specifically, this decrease occurs in the material even when the maximum temperature is lower than the monoclinic-tetragonal zirconia transformation (~1100 °C). This latter observation confirms that the zirconia phase change, either in the matrix or in the aggregates, does not play a major role in microcracking. The last possible origin for microcracking lies in the differential volume changes between the matrix and MZ aggregates during cooling. This option is supported by the dilatometric studies of the matrix (Fig. 6) and of the MZ aggregates (Fig. 7b) that show a radically different behavior. In addition, a very low CTE of $3.3 * 10^{-6}$ /°C was measured during cooling between 600 and 200 °C. As the CTE of the matrix ($7.0 *10^{-6}$ /°C) is more than twice this value hence during cooling, the matrix tends to contract more than the mullite-zirconia aggregates, which should lead to damage in the form of radial cracks, according to the model developed by Fogaing et al. [7]. Dilatometric measurements also show that:

- Alumina aggregates and the matrix have close CTE values which explains the fact that the alumina aggregates do not have a major contribution to microcracking in the refractory.
- The difference of CTE between the mullite aggregates ($5.1 *10^{-6}$ /°C) and the matrix ($7.0 *10^{-6}$ /°C) also appears to be the main cause of microcracking in 'mat_Mul'.

These results indicate that the main contributions to microcracking in the studied material is the CTE difference between the matrix and the mullite-zirconia aggregates.

The second temperature cycles in HMOE and hot strength provide extra information and allow showing the reversibility of the microcracking phenomenon. From 900° to 1000°C, the hot strength abruptly decreases due to the liquid phases present in the material. As a consequence, the previously created microcracks tend to close by differential thermal expansion effect or to heal thanks to their filling by liquid phases in their soft/liquid state [7]. This closing phenomena might explain the observed lower expansion during the second heating as compared to the first one as the matrix can, by a thermal expansion effect, close the existing microcracks. The observed effective macroscopic CTE will then be lower than for an uncracked sample. This assumption is validated by the HMOE rise from 900° to 1200°C in the second cycle. The completion of the sintering phenomenon might also partly explain this rise. However, after two cycles, the sintering phenomenon was completed and, during the third cycle (Fig. 8), a similar rise was observed from 900° to 1200°C, this time fully attributed to microcracks closing and healing. During cooling, the HMOE and the hot strength firstly increase until 1000 °C due to the solidification of liquid phases, but to a lesser extent than during the first cooling phase. It indicates that the microcracks created during the first cooling have been only partially closed/healed during this second cycle. For lower temperatures, the MOE and the hot strength continuously decrease and an inflection is observed in the dilatometry curve around 750 °C, similarly to the first cycle, evidencing crack opening. The third MOE cycle is similar to the second one, which shows that microcracking in this AMZ refractory is mainly reversible between the second cycle and the successive ones.

5. Conclusion

A high alumina cement-based refractory castable was prepared and characterized. The material consisted in alumina and mullite-zirconia aggregates (millimeter range in size) embedded in an alumina, zirconia and silica matrix with a CAC binder. Elastic modulus, strength and dilatometry measurements during successive thermal cycles were performed and analyzed to improve the understanding of the thermomechanical behavior of the material. Three main phenomena occur during thermal treatment of the material:

- Dehydration at low temperatures, in the first temperature cycle, due to cement hydrates decomposition.
- Liquid phase sintering during heating, mainly in the first temperature cycle.
- Microcracking during cooling.

To investigate the origin of the latter phenomenon, the matrix (particles smaller than 200 μm) and the aggregates (particles larger than 200 μm) of the refractory ceramic were separately studied. In addition, specific formulations with only alumina aggregates and with mullite-zirconia aggregates replaced by mullite ones were investigated. It was demonstrated that, although the zirconia tetragonal to monoclinic phase change leads to volume changes that are noticeable in the behavior of the refractory, microcracking is mainly driven by the difference of coefficients of thermal expansion between the matrix and the mullite-zirconia aggregates. This result was confirmed by the measure of the thermal expansion mismatch of the mullite-zirconia aggregates

($3.3 *10^{-6}$ /°C) and the matrix ($7.0 *10^{-6}$ /°C). In addition, it was shown that the microcracking effect was nearly fully reversible by crack closing (thanks to differential thermal expansion) or healing (filling by soft liquid phases) during a second heating cycle.

This work provided a detailed understanding of the mechanisms occurring during a thermal treatment of this refractory material. However, more knowledge could be useful for its optimization for industrial applications. For instance, the effect of the presence of thermally induced microcracks on the thermal shock resistance will be studied in the future. Furthermore, another medium-term perspective of this work is an exhaustive study of the evolution of the microstructure during a thermal treatment of the material and the links with its mechanical behavior.

Declaration of Competing Interest

The authors declare that they have no known competing financial interests or personal relationships that could have appeared to influence the work reported in this paper.

Acknowledgments

The authors thank all teams of Saint-Gobain Research Provence for the support in the experimental work, especially SEFPRO and the LAP (Laboratoire d'Application Physique). This research has been funded by Saint Gobain Group and Association Nationale de la Recherche et de la Technologie (ANRT) under CIFRE grant 2021/1421.

Appendix A. Supporting information

Supplementary data associated with this article can be found in the online version at doi:10.1016/j.jeurceramsoc.2023.09.051.

References

[1] Terminology for refractories, *ISO 836:2001*, 2022.
[2] J. Roy, S. Chandra, S. Maitra, Nanotechnology in castable refractory, Ceram. Int. vol. 45 (1) (2019) 19–29.
[3] W. Lee, W. Vieira, S. Zhang, K.G. Ahari, H. Sarpoolaky, C. Parr, Castable refractory concretes, Int. Mater. Rev. vol. 46 (3) (2001) 145–167.
[4] P. Boch, T. Chartier, Tape casting and properties of mullite and zirconia–mullite ceramics, J. Am. Ceram. Soc. vol. 74 (10) (1991) 2448–2452.
[5] S. Prochazaka, J.S. Wallace, N. Claussen, Microstructure of sintered mullite-zirconia composites, J. Am. Ceram. Soc. vol. 66 (8) (1983) C-125–C-127.
[6] C. Wolf, R. Kauermann, H. Hübner, J. Rodrigues, V. Pandolfelli, Effect of mullite-zirconia additions on the creep behaviour of high-alumina refractories, J. Eur. Ceram. Soc. vol. 15 (9) (1995) 913–920.
[7] E. Yeugo Fogaing, Caractérisation à haute température des propriétés d'élasticité de réfractaires électrofondus et de bétons réfractaires, Limoges (2006).
[8] N. Tessier-Doyen, J. Glandus, M. Huger, Untypical Young's modulus evolution of model refractories at high temperature, J. Eur. Ceram. Soc. vol. 26 (3) (2006) 289–295.
[9] M. Huger, T. Ota, N. Tessier-Doyen, P. Michaud, T. Chotard, Microstructural effects associated to CTE mismatch for enhancing the thermal shock resistance of refractories, in: IOP Conference Series: Materials Science and Engineering, vol. 18, IOP Publishing,, 2011, 222002.
[10] Z. Hashin, S. Shtrikman, A variational approach to the theory of the elastic behaviour of multiphase materials, J. Mech. Phys. Solids vol. 11 (2) (1963) 127–140.
[11] M. Huger , 2008. Elasticité à haute température de matériaux céramiques: effet des hétérogénéités.
[12] M.G. Kakroudi, E. Yeugo-Fogaing, C. Gault, M. Huger, T. Chotard, Effect of thermal treatment on damage mechanical behaviour of refractory castables: comparison between bauxite and andalusite aggregates, J. Eur. Ceram. Soc. vol. 28 (13) (2008) 2471–2478.
[13] F. Asadi, D. André, S. Emam, P. Doumalin, M. Huger, Numerical modelling of the quasi-brittle behaviour of refractory ceramics by considering microcracks effect, J. Eur. Ceram. Soc. vol. 42 (3) (2022) 1149–1161.
[14] D. Boccaccini, M. Romagnoli, E. Kamseu, P. Veronesi, C. Leonelli, G.C. Pellacani, Determination of thermal shock resistance in refractory materials by ultrasonic pulse velocity measurement, J. Eur. Ceram. Soc. vol. 27 (2–3) (2007) 1859–1863.
[15] C. Ferrari, J. Rodrigues, Microstructural features of alumina refractories with mullite-zirconia aggregates, Bol. Soc. Esp. Ceram. Vidr. vol. 42 (1) (2003) 15–20.
[16] T. Chotard, J. Soro, H. Lemercier, M. Huger, C. Gault, High temperature characterisation of cordierite–mullite refractory by ultrasonic means, J. Eur. Ceram. Soc. vol. 28 (11) (2008) 2129–2135, https://doi.org/10.1016/j.jeurceramsoc.2008.02.029.
[17] J.K. Winter, S. Ghose, Thermal expansion and high-temperture crystal chemistry of the Al 2 SiO 5 polymorphs, Am. Mineral. vol. 64 (5–6) (1979) 573–586.
[18] M. Mouiya, N. Tessier-Doyen, Y. Tamraoui, J. Alami, M. Huger, High temperature thermomechanical properties of a microcracked model refractory material: A silica-doped aluminium titanate, Ceram. Int. (2023).
[19] M.G. Kakroudi, E. Yeugo-Fogaing, M. Huger, C. Gault, T. Chotard, Influence of the thermal history on the mechanical properties of two alumina based castables, J. Eur. Ceram. Soc. vol. 29 (15) (2009) 3197–3204.
[20] Y. Moriya, A. Navrotsky, High-temperature calorimetry of zirconia: heat capacity and thermodynamics of the monoclinic–tetragonal phase transition, J. Chem. Thermodyn. vol. 38 (3) (2006) 211–223.
[21] D. Simeone, D. Gosset, J. Bechade, A. Chevarier, Analysis of the monoclinic–tetragonal phase transition of zirconia under irradiation, J. Nucl. Mater. vol. 300 (1) (2002) 27–38.
[22] C. Patapy, C. Gault, M. Huger, T. Chotard, Acoustic characterization and microstructure of high zirconia electrofused refractories, J. Eur. Ceram. Soc. vol. 29 (16) (2009) 3355–3362.
[23] E.Y. Fogaing, Y. Lorgouilloux, M. Huger, C. Gault, Young's modulus of zirconia at high temperature, J. Mater. Sci. vol. 41 (2006) 7663–7666.
[24] E.Y. Fogaing, M. Huger, C. Gault, Elastic properties and microstructure: study of two fused cast refractory materials, J. Eur. Ceram. Soc. vol. 27 (2–3) (2007) 1843–1848.
[25] A. Sibil, T. Douillard, C. Cayron, N. Godin, M. R'mili, G. Fantozzi, Microcracking of high zirconia refractories after t→ m phase transition during cooling: An EBSD study, J. Eur. Ceram. Soc. vol. 31 (9) (2011) 1525–1531.
[26] R. Salomão, M.R. Ismael, V.C. Pandolfelli, Hydraulic binders for refractory castables: mixing, curing and drying, Ceram. Forum Int. vol. 84 (9) (2007) 103–108.
[27] N.H. Golshan, H. Sarpoolaky, A. Souri, Microstructure and properties of colloidal silica bonded magnesite castable refractories, Iran. J. Mater. Sci. Eng. vol. 8 (1) (2011) 25–31.
[28] B. Bezerra, A. Luz, V. Pandolfelli, Novel drying additives and their evaluation for self-flowing refractory castables, Ceram. Int. vol. 46 (3) (2020) 3209–3217.
[29] J. Poirier, "Les céramiques réfractaires de l'élaboration aux propriétés d'emploi," 2011.
[30] R. Sarkar, Binders for refractory castables: an overview, Inter. -Int. Ceram. Rev. vol. 69 (2020) 44–53.
[31] N.L. Emmanuel Nonnet, Philippe Boch, Elastic Properties of High Alumina Cement Castables from Room Temperature to 1600C, J. Eur. Ceram. Soc. (1998), https://doi.org/10.1016/S0955-2219(98)00255-6.
[32] F. Simonin, C. Olagnon, S. Maximilien, G. Fantozzi, L.A. Diaz, R. Torrecillas, Thermomechanical behavior of high-alumina refractory castables with synthetic spinel additions, J. Am. Ceram. Soc. vol. 83 (10) (2000) 2481–2490, https://doi.org/10.1111/j.1151-2916.2000.tb01579.x.
[33] M.A. Braulio, G.G. Morbioli, J. Medeiros, J.B. Gallo, V.C. Pandolfelli, Nano-bonded wide temperature range designed refractory castables, J. Am. Ceram. Soc. vol. 95 (3) (2012) 1100–1104, https://doi.org/10.1111/j.1551-2916.2011.05053.x.
[34] J.-M. Auvray, C. Gault, M. Huger, Evolution of elastic properties and microstructural changes versus temperature in bonding phases of alumina and alumina–magnesia refractory castables, J. Eur. Ceram. Soc. vol. 27 (12) (2007) 3489–3496, https://doi.org/10.1016/j.jeurceramsoc.2007.01.016.
[35] I. NV. "Leading world wide reference partner in dynamic material testing instruments." ⟨https://imce.eu/⟩ (accessed 2023).
[36] Polytec. "Vibrométrie laser Doppler." ⟨https://www.polytec.com/fr/vibrometrie/technologie/vibrometrie-laser-doppler⟩ (accessed 2023).
[37] A.K. Swarnakar, O. Van der Biest, J. Vanhellemont, Determination of the Si Young's modulus between room and melt temperature using the impulse excitation technique, Phys. Status Solidi (C.) vol. 11 (1) (2014) 150–155.
[38] W. Pabst, E. Gregorová, D. Malangré, J. Hostaša, Elastic properties and damping behavior of alumina–zirconia composites at room temperature, Ceram. Int. vol. 38 (7) (2012) 5931–5939.
[39] W.J. Campbell, C. Grain, Thermal expansion of alpha-alumina, Adv. X-ray Anal. vol. 5 (1961) 244–256.
[40] N.M. Rendtorff, L.B. Garrido, E.F. Aglietti, Thermal shock behavior of dense mullite–zirconia composites obtained by two processing routes, Ceram. Int. vol. 34 (8) (2008) 2017–2024.
[41] M. Ghassemi Kakroudi, "Comportement thermomécanique en traction de bétons réfractaires: influence de la nature des agrégats et de l'histoire thermique," PhD, University of Limoges, France, 2007.
[42] W. Yuan, Q. Zhu, C. Deng, H. Zhu, The effect of the glass phase on modulus of rupture of high alumina refractories, J. Ceram. Sci. Technol. vol. 6 (3) (2015) 215–220.
[43] J.-M. Auvray, Elaboration et caracterisation a haute temperature de betons refractaires a base d'alumine spinelle, Univ. Limoges (2003).
[44] G.W. SCHERERA, Sintering with rigid inclusions, J. Am. Ceram. Soc. vol. 70 (10) (1987) 719–725.
[45] M.W. Weiser, L.C. De Jonghe, Inclusion size and sintering of composite powders, J. Am. Ceram. Soc. vol. 71 (3) (1988) C-125–C-127.

[46] A. Evans, Considerations of inhomogeneity effects in sintering, J. Am. Ceram. Soc. vol. 65 (10) (1982) 497–501.
[47] O. Sudre, F.F. Lange, Effect of inclusions on densification: I, microstructural development in an Al2O3 matrix containing a high volume fraction of ZrO2 inclusions, J. Am. Ceram. Soc. vol. 75 (3) (1992) 519–524.
[48] C. Patapy, et al., Mechanical behavior characterization of high zirconia fused-cast refractories at high temperature: Influence of the cooling stage on microstructural changes, J. Eur. Ceram. Soc. vol. 32 (15) (2012) 3929–3939.